



Lithostratigraphy and paleoceanography in the Chukchi Rise of the western Arctic Ocean since the last glacial period



Kwangkyu Park ^{a, b}, Ken'ichi Ohkushi ^c, Hyen Goo Cho ^d, Boo-Keun Khim ^{a, *}

^a Department of Oceanography, Pusan National University, 46241 Busan, Republic of Korea

^b Division of Polar Paleoenvironment, Korea Polar Research Institute, 21990 Incheon, Republic of Korea

^c Graduate School of Human Development and Environment, Kobe University, Kobe 657-8501, Japan

^d Department of Geology and Research Institute of Natural Science, Gyeongsang National University, Jinju 52828, Republic of Korea

ARTICLE INFO

Article history:

Received 19 January 2016

Received in revised form

16 December 2016

Accepted 24 January 2017

Available online 26 January 2017

Keywords:

Lithostratigraphy

Paleoceanography

Geochemical proxies

Provenance

Chukchi Rise

ABSTRACT

Paleoceanographic multi-proxies were investigated from two piston cores PC01 and PC04, along with two pilot cores PL01 and PL04, collected from the Chukchi Rise in the western Arctic Ocean during the R/V Mirai Cruise MR09-03. Both cores were composed of three lithologic units (Unit I: the Holocene brownish sandy mud, Unit II: the deglacial IRD layer, and Unit III: the glacial and gray thick mud with intervened IRD layers). The age estimate of the core units were decided by AMS ¹⁴C dates and confirmed by the correlation of the geochemical properties and ice-rafted debris (IRD) pattern with the well-dated core (P2) in the study area. The geochemical, isotopic, and mineralogical properties indicate different paleoceanographic conditions of three lithologic units in the Chukchi Rise: low primary production during the glacial period (Unit III), high terrigenous contribution during the deglacial period (Unit II), and increase in diatom productivity during the late Holocene (Unit I). In particular, most IRDs were specified as detrital carbonates (calcites and dolomites) by SEM-EDS examination. The sediment source from the northern North America and the transport pathway by the Beaufort Gyre were confirmed by the isotopic signature of bulk IRDs and high kaolinite content of fine-grained particles.

© 2017 Elsevier B.V. and NIPR. All rights reserved.

1. Introduction

The Arctic Ocean is one of the most remarkable areas in the world with regard to the current global climate change. Over the last century, the Earth has warmed by 0.56–0.92 °C, but an approximately 3 °C increase has been recorded in the Arctic regions (IPCC, 2007). In addition, based on the instrumental record over the last 30 years, the increase in the Arctic temperature is almost double that of the global average. Such recent temperature increases are accompanied with sea ice melting (Stroeve et al., 2012), ice sheet retreat (Abdalati and Steffen, 2001), increase in river runoff (Peterson et al., 2002), coastal erosion enhancement (Jones et al., 2009), and permafrost degradation (Lawrence et al., 2008). Shimada et al. (2006) reported that these environmental changes would become intensified and especially distinct in the western Arctic Ocean.

The Arctic cryosphere is linked closely to the climate system

regarding solar radiation absorption and global ocean circulation (Callaghan et al., 2011). Because ice sheets and sea ice are the cryosphere's principal components, information on their development and evolution is essential for understanding the role of the Arctic Ocean in global climate change. The changes in the ice sheets and sea ice have a direct influence on the sedimentary environment. Hence, the environmental changes in the Arctic Ocean are generally recorded from the marine sediments (e.g., Phillips and Grantz, 2001; Backman et al., 2004; Darby et al., 2006; Stein et al., 2010; Polyak and Jakobsson, 2011). Thus, it is important to examine the marine sediments containing ice-rafted debris (IRD), which is transported mainly by icebergs and/or sea ice. On the other hand, there is still limited information on marine sedimentation in the Arctic Ocean, because of the insufficient sediment core collection due to the thick multiyear (or perennial) sea ice and short summer time, particularly in the western Arctic Ocean. Furthermore, sediment records were difficult to interpret precisely because of the low sedimentation rates (e.g., Darby et al., 1997; Backman et al., 2004; Polyak et al., 2009), erosional perturbations by glacier (e.g., Polyak et al., 2001, 2007; Jakobsson et al., 2010; Dove et al., 2014), and chronological inconsistencies (e.g., Backman

* Corresponding author.

E-mail address: bkkhim@pusan.ac.kr (B.-K. Khim).

et al., 2008; Stein et al., 2010). In the case of the chronological problems, different arguments regarding age dating and inter-core correlation require the complete establishment of stratigraphy in the Arctic Ocean (Stein et al., 2010).

The Chukchi Rise, which is an extension of the Chukchi Shelf, is located about 900 km away from the Bering Strait (Fig. 1). The Chukchi Shelf was exposed subaerially during the glacial periods and connected to the Bering Sea, forming the Beringian. At the same time, land masses near the Arctic Ocean such as North America, Greenland, and northwestern Eurasia were occupied by continental ice sheets and several continental shelves were glaciated (Ehlers and Gibbard, 2007; Jakobsson et al., 2013). These glaciomarine environments played an important role in governing sediment transport and deposition in the Arctic Ocean by various processes such as glacial erosion (e.g., Polyak et al., 2007; Dove et al., 2014), mass (or debris) flow (e.g., Grantz et al., 1996), suspension settling (e.g., Cowan et al., 1999), and iceberg discharge (e.g., Darby et al., 2002). Most research on sedimentary processes under the glaciomarine environment were restricted to the Atlantic side of the Arctic Ocean (e.g., Dowdeswell and Ó Cofaigh, 2002 and references therein); comparative studies in the Pacific side of the Arctic Ocean are lacking. Moreover, recent studies on glaciomarine sediments in the Arctic Ocean have focused mainly on the topographic highs, such as submarine ridges and plateaus (e.g., Polyak et al., 2004; O'Regan et al., 2008; Jakobsson et al., 2008, 2010). More studies on bedform mapping and stratigraphic investigation will be needed to reveal the timing and scale of both continental and marine-based ice sheets. The Chukchi Rise in the western Arctic Ocean might be one important area characterized by glaciomarine sedimentary environment, which reflects the changes in the Arctic cryosphere through the glacial-interglacial cycles.

In this study, various paleoceanographic indicators (biogenic opal content, total organic carbon (TOC) content, TOC/total nitrogen (TN) (C/N) ratio, total inorganic carbon (TIC) content, carbon isotope of organic matter ($\delta^{13}\text{C}_{\text{org}}$), IRD abundance, carbon and oxygen isotopes of bulk carbonates ($\delta^{13}\text{C}_{\text{carb}}$ and $\delta^{18}\text{O}_{\text{carb}}$), clay minerals, and grain size) of the sediment cores collected from the Chukchi Rise in the western Arctic Ocean were analyzed. The main

objectives of our study are to establish the lithostratigraphy of the core sediments based on these multi-proxies and to reconstruct the paleoenvironmental and paleoceanographic changes in the Chukchi Rise.

2. Material and methods

Two piston cores PC01 (587.4 cm long, 75°28.1' N, 165°40.4' W, 558 m deep) and PC04 (927.8 cm long, 74°26.3' N, 165°44.3' W, 370 m deep) along with pilot cores PL01 (30 cm long) and PL04 (22 cm long) were collected from the Chukchi Rise by R/V Mirai of Japan Agency for Marine–Earth Science and Technology during the MR09-03 cruise in 2009 (Fig. 1). After splitting each section of the piston and pilot cores into working and archive halves, core color reflectance (CCR; L^* , a^* , and b^*) was measured onboard from the archive half using a Konica Minolta CM-700d spectrometer. Soft X-ray photographs were also taken using a SOFTEX PRO-TEST 150 to observe the sedimentary structures and to count IRD ($>150\ \mu\text{m}$) particles. For the laboratory analyses, the core sediments were subsampled at 1–2 cm intervals (2 cm for piston cores and 1 cm for pilot cores) and some of them were ground after freeze-drying for geochemical analyses. The sample selection for the measurement of other proxies ($\delta^{13}\text{C}_{\text{org}}$, $\delta^{13}\text{C}_{\text{carb}}$, $\delta^{18}\text{O}_{\text{carb}}$, grain size, and clay minerals) was decided after the recognition of geochemical variations.

2.1. Geochemical (biogenic opal, TIC, TOC, and C/N ratio) measurement

Geochemical properties were measured at 146 horizons for core PC01, 31 horizons for core PL01, 164 horizons for core PC04, and 21 horizons for core PL04. Biogenic Si (Si_{BIO}) content was measured using the molybdate blue spectrophotometric method following the wet-alkaline sequential extraction method modified from Mortlock and Froelich (1989). Subsequently, the biogenic opal content was calculated by multiplying Si_{BIO} by 2.4 (Mortlock and Froelich, 1989). The analytical error of Si_{BIO} content was less than $\pm 1\%$.

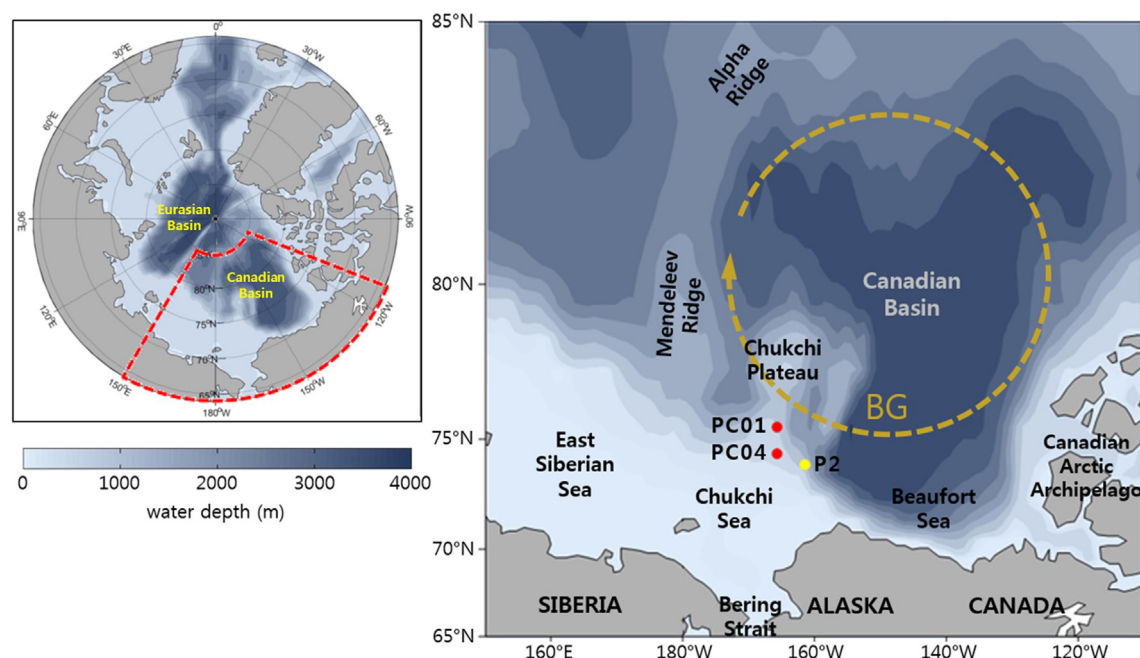


Fig. 1. Locations of two cores (PC01 and PC04) used in this study and core P2 studied by Polyak et al. (2007). The dashed arrow indicates the anticyclonic Beaufort Gyre (BG).

$$\text{Biogenic opal (\%)} = \text{Si}_{\text{BIO}}(\%) \times 2.4 \quad (2.1)$$

TIC content was measured using a UIC CO₂ Coulometer CM5014. The analytical error of TIC was $\pm 1.0\%$. TC and TN were measured using an elemental analyzer Flash 2000. The analytical errors of TC and TN were less than $\pm 0.1\%$ and $\pm 0.01\%$, respectively. TOC was calculated as the difference between TC and TIC. C/N ratio was calculated by TOC/TN.

$$\text{TOC (\%)} = \text{TC (\%)} - \text{TIC (\%)} \quad (2.2)$$

2.2. IRD and grain size analyses

IRD ($>150 \mu\text{m}$) was counted from the soft X-ray photographs at 2-cm intervals in both cores, PC01 and PC04. The IRD abundance is expressed as the number of IRD per unit volume ($\#/\text{cm}^3$). At the same horizons of clay mineral analysis (subsection 2.4), the bulk sediments were sieved through a 63- μm mesh size. The IRDs larger than 500 μm selected from the remaining coarse grains were analyzed to identify their constituents and compositions by scanning electron microscopy (SEM) - energy dispersive X-ray spectrometry (EDS) analyzer (SEM 515 & PV 9800) at Korea Institute of Ocean Science and Technology (KIOST).

Grain size was analyzed at 11 horizons for the core PC01 using a Laser Diffraction Particle Analyzer S3500 at the Korea Institute of Geology and Mineral Resources. For pretreatment, the organic matter of the dried bulk sediments was removed using a 6% hydrogen peroxide solution. Mean grain size was calculated using the Gradistat (Blott and Pye, 2001).

2.3. Stable isotope analyses

$\delta^{13}\text{C}_{\text{org}}$ value of sedimentary organic matter was measured from 32 horizons for the core PC01, 5 horizons for core PL01, 37 horizons for core PC04, and 4 horizons for core PL04 using the Europa Scientific 20-20 Elemental Analyzer-Isotopes Ratio Mass Spectrometer (IRMS) at Iso-Analytical Ltd (UK). Precision for $\delta^{13}\text{C}_{\text{org}}$ value is $\pm 0.1\text{‰}$. $\delta^{18}\text{O}_{\text{carb}}$ and $\delta^{13}\text{C}_{\text{carb}}$ values of the bulk carbonates were also measured from 14 intervals for core PC01, 8 intervals for core PL01, and 21 intervals for core PC04 at Iso-Analytical Ltd (UK). The conventional delta notation is per mil deviation from the Vienna Pee Dee Belemnite (VPDB) for the carbon and oxygen isotopes. Precisions are $\pm 0.1\text{‰}$ for the carbon isotope and $\pm 0.2\text{‰}$ for the oxygen isotope, respectively.

2.4. Clay mineral analysis

Clay mineral compositions were measured on 30 horizons for core PC01, 3 horizons for core PL01, 29 horizons for core PC04, and 3 horizons for core PL04. The organic matter of bulk sediment was removed using a 6% hydrogen peroxide solution. After

sieving through a 63 μm mesh, the clay particles ($<2 \mu\text{m}$) were extracted by a settling technique based on Stoke's Law. The extracted clays were applied to the glass slide in their orientation (Stokke and Carson, 1973) and air-dried. The untreated samples were analyzed by X-ray diffraction (XRD) using PANanalytical X'Pert PRO and they were analyzed again after ethylene glycol-saturation at 60 °C for 24 h (Brunton, 1955) at KIOST. Relative contents of the major clay minerals (illite (10 Å), smectite (17 Å), and kaolinite and chlorite (7.1 Å)) were calculated semi-quantitatively using the scheme reported by Biscaye (1965). The division of kaolinite and chlorite was in proportion to the relative areas of their 002 (3.58 Å) and 004 (3.54 Å) peaks, respectively (Biscaye, 1964).

2.5. AMS ¹⁴C dating

Seven accelerator mass spectrometry (AMS) ¹⁴C dates were measured using the sedimentary organic matters of core PC01 at Rafter Radiocarbon Laboratory, National Isotope Center, New Zealand (Table 1). Radiocarbon dates were calibrated into calendar ages using CALIB 6.0.0 (Marine09; Reimer et al., 2009) with a reservoir effect correction ($\Delta R = 0$), because the reservoir ages in the Arctic waters are uncertain (Darby et al., 1997; Polyak et al., 2007; Hanslik et al., 2010). Thus, the calibrated ¹⁴C ages are believed to be their maximum values, because bulk organic matter could contain old carbon.

3. Results

3.1. Core-top compensation

The CCR (L^* , a^* , and b^*) of piston cores were compared with those of the pilot cores, because the top part of the piston corer is generally lost during the core retrieval process, whereas pilot corers preserve the complete sediment-water interface of the core-top. The CCR patterns between the top parts of the piston and pilot cores were not similar (Fig. 2), which confirms that some core-top sediments in the piston core were missing. Thus, the lost part of piston core was substituted by the pilot core sediments based on matching of the CCR between the two cores (Fig. 2). As a result, top-loss lengths for cores PC01 and PC04 were most likely to be 15 cm and 20 cm, respectively. Finally, the composite depths (602.4 cm for PC01/PL01 and 967.2 cm for PC04/PL04) were used throughout this study.

3.2. Lithologic units and their age estimates

According to visual description of lithology and sediment color, both cores were divided distinctly into three lithologic units: Units I, II, and III in descending order (Fig. 3). Unit I (from 65 cm to the core top for core PC01/PL01 and from 171 cm to the core-top for

Table 1
AMS ¹⁴C data of core PC01. OM: organic matter.

Composite depth (cm)	Material	Measured ¹⁴ C age (yr BP)	Calibrated ¹⁴ C age (2 σ range) (yr BP)	$\delta^{13}\text{C}_{\text{org}}$ (‰)	GNS code
65–67	OM	7462 \pm 30	7918.5 \pm 73.5	–22.0	NZA 36530
119–121	OM	29 860 \pm 260	34 033 \pm 646	–24.4	NZA 36546
169–171	OM	29 560 \pm 260	33 856.5 \pm 709.5	–24.8	NZA 36531
217–219	OM	27 860 \pm 210	31 674.5 \pm 451.5	–24.3	NZA 36525
325–327	OM	26 471 \pm 148	28 839.5 \pm 312.5	–25.2	NZA 51071
437–439	OM	25 188 \pm 128	27 812 \pm 401	–25.0	NZA 51072
545–547	OM	25 275 \pm 130	27 867 \pm 379	–24.9	NZA 51073

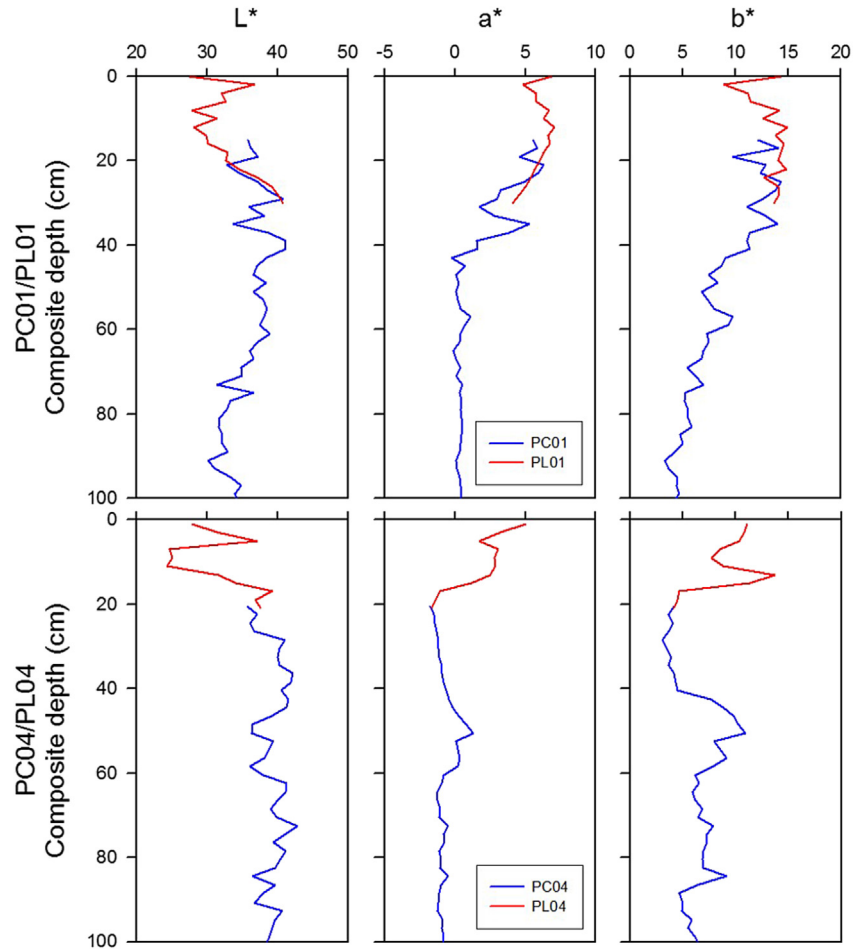


Fig. 2. Comparison of the core color indices (L^* , a^* and b^*) between the uppermost part of the piston cores and the pilot cores for the construction of composite cores. (For interpretation of the references to colour in this figure legend, the reader is referred to the web version of this article.)

core PC04/PL04) was composed of dark brown to grayish olive silty clay with a few scattered IRD patches and some bioturbated structures (Figs. 3 and 4). Unit II (from 105.0 cm to 65.0 cm for core PC01/PL01 and from 476.2 cm to 171.0 cm for core PC04/PL04) was characterized by abundant IRD (Figs. 3 and 4). Unit II in PC04/PL04 was featured by hundreds of lamina which has an alternation of fine-grained and coarse-grained sediment layer (Fig. 4). Unit III (from the core bottom to 105.0 cm for core PC01/PL01 and from the core bottom to 476.2 cm for core PC04/PL04) was composed of massive or laminated mud with dark olive gray colored intermittently containing a couple of IRD layers (Figs. 3 and 4).

Although AMS ^{14}C ages of this study are believed to be old because of containing old carbon in the bulk organic matter, these ages are sufficient to support the lithologic division at the interglacial-glacial scale (Fig. 3). An AMS ^{14}C dating (7.9 ka) in Unit I represents Holocene sedimentation (Fig. 3; Table 1), and a comparison of the sediment properties (brownish color and low to moderate sand content) with the other cores in the Arctic Ocean confirms the age estimate (Polyak et al., 2007; Wang et al., 2010). The AMS ^{14}C ages of Unit III in core PC01/PL01 were in the range between 27.8 and 34.0 ka (Table 1), indicating that the age of Unit III was estimated as the last glacial period, although they were not in chronological order (Fig. 3). No direct AMS ^{14}C dating was performed in Unit II due to the absence of datable materials. Considering the distinct lithology and AMS ^{14}C date (7.9 ka) of the bottom part of Unit I, Unit II appears to have been deposited during the pre-Holocene period. Polyak et al. (2007) reported that core P2 (348 cm

long, $73^\circ 57.3' \text{ N}$, $161^\circ 31.7' \text{ W}$, 368 m deep) in the Chukchi Borderland preserved the Holocene mud, the gray mud with IRD layers, and diamicton, among which the gray mud with the IRD layers was dated to be approximately 13–14 ka. The lithostratigraphic correlation showed that Unit II in the present study might be equivalent to the gray mud with IRD layer of the dated core P2, which signifies that Unit II represents the pre-Holocene and the last deglacial period. This also confirms that Unit III represents the last glacial period. Therefore, Units I, II, and III of both cores most likely correspond to the middle to late Holocene, the last deglacial period, and the last glacial period, respectively.

Based on the assumed age estimation, sedimentation rates are calculated as possible for each unit of PC01. Despite single age dating point in Unit I, this age represents the bottom age of Unit I. Thus, the sedimentation rate of Unit I is in the range of 8.1–9.3 cm/ky (7918 ± 73.5 years for 65 cm; Table 1). Sedimentation rate of Unit II is also possible when considering the terminal timing of the last glaciation (approximately 13–14 ka) (Polyak et al., 2007), corresponding to the boundary between Units II and III. In this regard, the sedimentation rate of Unit II is estimated as 6.7–8.0 cm/ky (5000–6000 years for 40 cm). Sedimentation rate of Unit III is more difficult to estimate due to the age reversal (Fig. 3; Table 1). However, although ages of Unit III were reversed sedimentation rate (approximately 30 cm/ky) was expected, assuming that the youngest age of Unit III is accepted. It means that this sedimentation rate seems to be minimum. In the same way applied to PC04, sedimentation rate of each unit is higher than PC01 (Fig. 3).

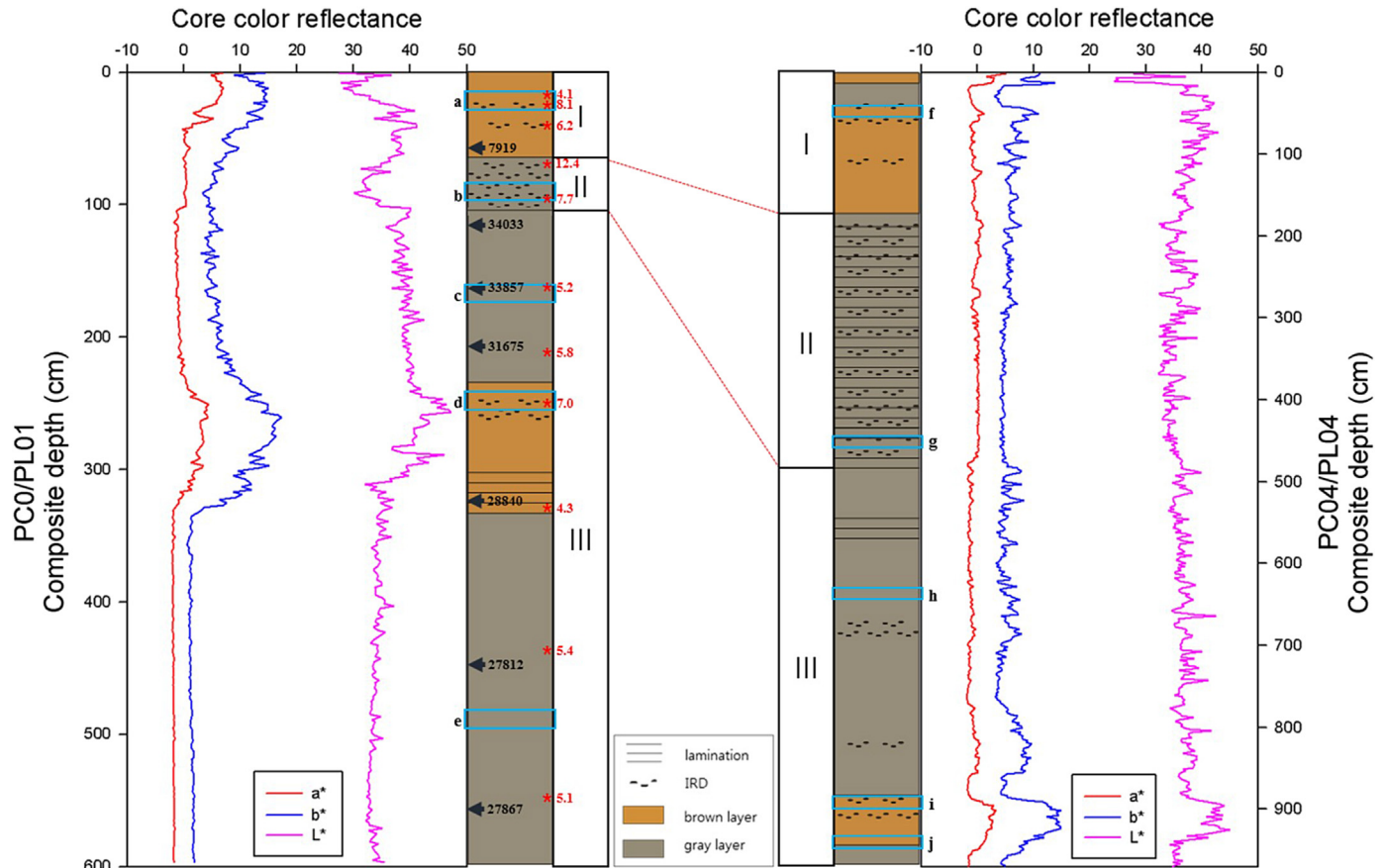


Fig. 3. Downcore profiles of the core color reflectance and lithostratigraphic units (Unit I, Unit II, Unit III) with the calibrated ^{14}C ages of composite core (PC01/PL01) and correlation of lithostratigraphic units between the two composite cores. Red asterisks (*) and numbers in core PC01 represent the sampling horizon for the grain size analysis and their mean grain size (μm). Grain size distributions were shown in S1. (For interpretation of the references to colour in this figure legend, the reader is referred to the web version of this article.)

3.3. Variations of paleoceanographic proxies

A range of paleoceanographic proxies such as sediment organic properties (TOC, C/N ratio, and $\delta^{13}\text{C}_{\text{org}}$), inorganic components (biogenic opal and TIC), bulk isotope composition ($\delta^{13}\text{C}_{\text{carb}}$ and $\delta^{18}\text{O}_{\text{carb}}$), particle properties (IRD and grain size), and clay minerals (smectite, illite, kaolinite and chlorite) highlights two important features. One is to support the lithologic division of cores PC01/PL01 and PC04/PL04 (Fig. 3), and another is to maintain the consistently similar downcore variations of these paleoceanographic multiproxies between the two cores (Figs. 4 and 5; Table 2).

The last glacial Unit III is characterized by low TOC content (0.1–0.6%) and C/N ratio (2.3–7.6), moderate $\delta^{13}\text{C}_{\text{org}}$ value (-25.3 – -24.0 ‰), low TIC content (up to 0.26%), and small mean grain size (4.3–5.8 μm ; fine silt); however, the intercalated IRD abundant layers show a high TOC content ($\sim 1.6\%$ for core PC04/PL04), high C/N ratio (~ 45.0), high TIC content (4.0%), and large mean grain size (7.0 μm) (Figs. 3, 5 and 6; Table 2). The $\delta^{18}\text{O}_{\text{carb}}$ and $\delta^{13}\text{C}_{\text{carb}}$ values of the three units were almost consistent ($\delta^{18}\text{O}_{\text{carb}}$ for -4.9 ‰ to -2.8 ‰ and $\delta^{13}\text{C}_{\text{carb}}$ for -2.6 ‰ to -1.0 ‰; Fig. 6; Table 2). On the other hand, an IRD horizon at 652.7 cm of core PC04/PL04 exhibited an abnormally low $\delta^{13}\text{C}_{\text{carb}}$ value (-14.7 ‰) and comparatively high $\delta^{18}\text{O}_{\text{carb}}$ value (3.9‰). Deglacial Unit II is distinguished from the other units by the very high TOC content (0.7–1.7%) and high C/N ratio (7.0–16.6), low $\delta^{13}\text{C}_{\text{org}}$ value (-26.5 – -25.5 ‰), high TIC content (0.06–0.83%), low $\delta^{18}\text{O}_{\text{carb}}$ values (ca. -5.0 ‰), and large mean grain size (7.7–12.4 μm) (Figs. 3, 5 and 6; Table 2). Holocene Unit I showed an upward increasing

TOC content (from 0.4 to 1.4%) and $\delta^{13}\text{C}_{\text{org}}$ values (from -26.7 to -22.1 ‰), as well as an upward decreasing C/N ratio (from 12.6 to 3.1), except for the IRD-enriched patches characterized by the high TIC content ($\sim 1.30\%$) and large mean grain size (6.2–8.1 μm) (Figs. 3, 5 and 6; Table 2).

The biogenic opal contents in both cores were similarly low and almost constant (3–7%) throughout the entire intervals, but a distinct increase in biogenic opal content up to 18% was observed at the upper part of Unit I in core PC04/PL04 (Fig. 5; Table 2). The relative contents of the major clay minerals were difficult to characterize in each unit (Fig. 7; Table 2). Nonetheless, the kaolinite contents appear to differentiate the lithologic units, showing that low kaolinite contents (9.8–14.8% for PC01 and 9.1–14.4% for PC04) corresponds to Units I and III and kaolinite contents are high (14.3–21.2% for PC01 and 13.4–23.9% for PC04) at all IRD layers (Fig. 7; Table 2). These IRD layers were also characterized by the high TIC content (up to 2.55%) (Fig. 6; Table 2). In particular, a SEM-EDS examination of these high TIC layers indicated that the main components of the IRD carbonate particles are detrital dolomite and calcite, not biogenic remnants (Fig. 8).

4. Discussion

4.1. Paleoceanographic changes in the Chukchi Rise

Our study shows that core sediments in the Chukchi Rise were divided temporarily into three stages in terms of lithological features and geochemical proxies; the mid-to-late Holocene, last

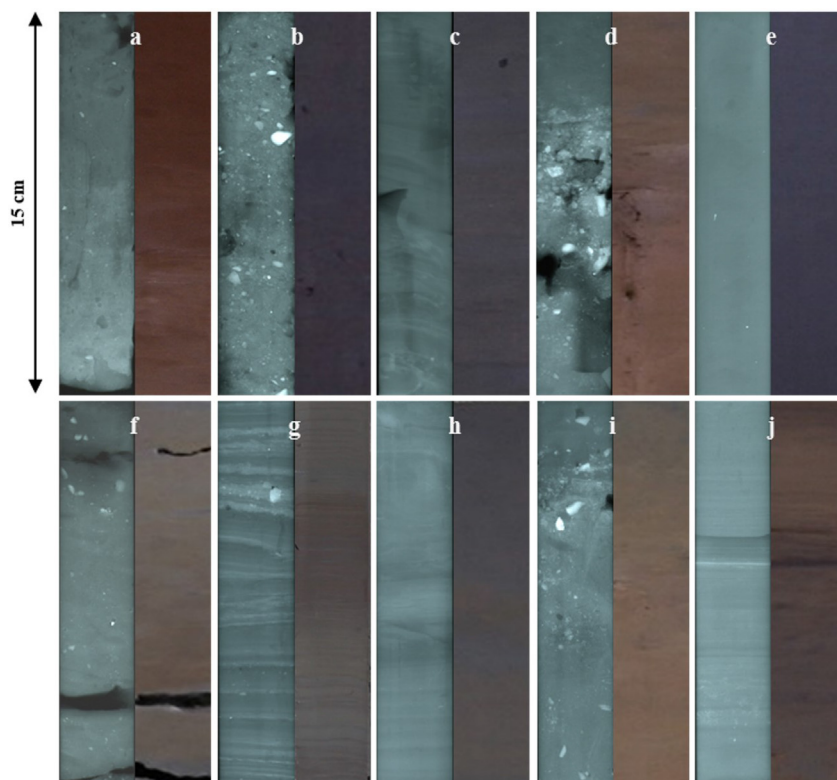


Fig. 4. Soft x-ray and core surface images of the two cores. The small letters indicate the position within the core as marked by blue box in Fig. 3. All vertical lengths were 15 cm long. (For interpretation of the references to colour in this figure legend, the reader is referred to the web version of this article.)

deglacial and last glacial corresponding to Units I, II, and III, respectively (Figs. 3, 5 and 6). In general, the Quaternary marine sediments of the Arctic Ocean can be typically divided into three different types; glacial, deglacial, and interglacial sediments (e.g., Polyak and Jakobsson, 2011). This sediment division is related

primarily to the variations of the depositional environment caused by glaciation and subsequent sea level change. During the glacial periods, when the sea level was low, the Arctic Ocean became much smaller due to the exposure of the shallow continental shelves where the glacial activity left coarse-grained diamictons, and

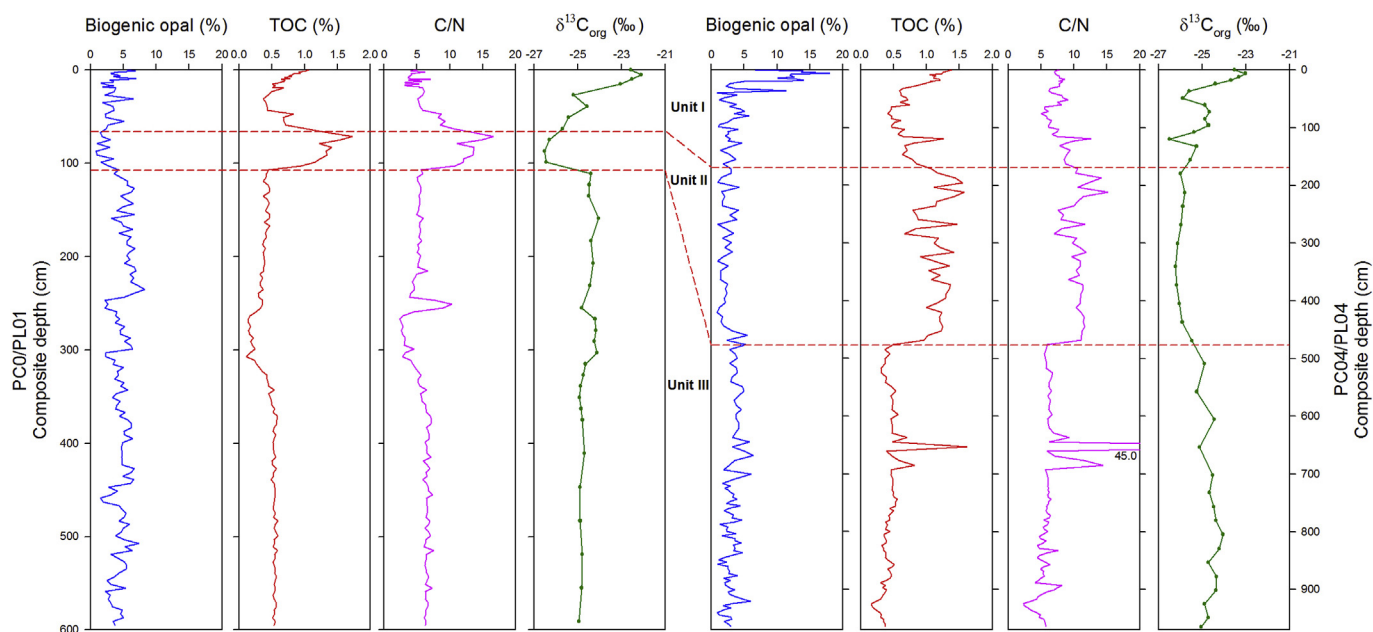


Fig. 5. Downcore profiles of the biogenic opal content, TOC (total organic carbon) content, C/N (TOC/total nitrogen, weight%) ratio and $\delta^{13}\text{C}_{\text{org}}$ value of sedimentary organic matter and their correlation between two composite cores.

Table 2
Summary of statistical results of geochemical and mineralogical data of PC01 and PC04. Please note that $\delta^{13}\text{C}_{\text{carb}}$ and $\delta^{18}\text{O}_{\text{carb}}$ values (-14.67‰ and 3.86‰ , respectively) for horizon of 552.7 cm (PC04) were excluded.

Proxies	Unit	PC01				PC04			
		Range		Average	Standard dev.	Range		Average	Standard dev.
		Min.	Max			Min.	Max		
Biogenic opal (%)	I	1.59	6.89	3.66	1.44	0.88	17.98	5.52	4.57
	II	0.84	3.46	1.97	0.96	0.91	5.42	2.26	1.01
	III	1.53	8.21	4.80	1.31	0.87	6.40	3.21	1.13
TOC (%)	I	0.37	1.06	0.68	0.19	0.40	1.38	0.80	0.29
	II	0.94	1.73	1.33	0.21	0.66	1.57	1.16	0.21
	III	0.11	0.59	0.44	0.12	0.16	1.61	0.43	0.16
C/N	I	3.11	10.60	5.44	1.90	5.02	12.58	7.53	1.36
	II	10.82	16.60	13.22	1.77	6.97	15.10	10.66	1.55
	III	2.35	10.27	5.76	1.30	2.35	44.98	6.23	4.33
$\delta^{13}\text{C}_{\text{org}}$ (‰)	I	-25.70	-22.11	-23.90	1.48	-26.49	-23.01	-24.74	1.01
	II	-26.52	-26.31	-26.43	0.11	-26.21	-25.46	-25.95	0.22
	III	-24.94	-22.11	-24.49	0.29	-25.24	-24.04	-24.63	0.34
TIC (%)	I	0.10	0.98	0.28	0.18	0.06	1.29	0.24	0.26
	II	0.19	0.83	0.64	0.23	0.07	0.69	0.30	0.17
	III	0.05	2.54	0.17	0.34	0.04	4.02	0.26	0.55
IRD (#/cm ³)	I	0	13.10	2.76	3.35	0	51.90	5.30	10.89
	II	1.90	128.10	54.85	30.96	0	39.05	3.18	6.32
	III	0	117.14	3.68	16.16	0	269.05	13.15	47.91
$\delta^{13}\text{C}_{\text{carb}}$ (‰)	I	-2.03	-1.02	-1.35	0.30	-1.36	-1.05	-1.12	0.12
	II	-4.34	-1.39	-2.33	0.90	-3.82	-1.78	-2.69	0.91
	III	-1.93	-1.01	-1.35	0.41	-2.56	-1.61	-2.17	0.34
$\delta^{18}\text{O}_{\text{carb}}$ (‰)	I	-5.07	-4.84	-4.96	0.09	-5.50	-4.09	-4.61	0.50
	II	-10.32	-6.38	-8.14	1.13	-5.48	-4.31	-5.00	0.50
	III	-4.69	-4.42	-4.59	0.12	-4.90	-2.80	-4.10	0.68
Smectite (%)	I	1.80	8.13	5.13	2.46	3.29	10.29	5.92	1.94
	II	4.20	8.72	6.78	1.73	3.22	7.26	5.60	1.63
	III	2.77	9.68	7.04	2.34	5.87	21.22	10.04	3.82
Illite (%)	I	53.93	61.81	59.07	2.60	51.59	64.02	58.23	3.67
	II	56.88	62.69	58.82	2.50	50.95	55.37	53.70	1.89
	III	60.80	68.10	63.91	1.81	57.13	63.53	60.22	2.15
Chlorite (%)	I	17.91	25.18	20.17	2.42	19.34	23.99	21.15	1.47
	II	15.79	17.76	16.72	0.79	19.28	21.25	20.26	0.71
	III	14.66	21.61	17.89	1.59	12.37	21.03	17.90	2.53
Kaolinite (%)	I	12.47	19.03	15.62	2.47	11.24	23.86	14.70	3.62
	II	12.80	21.23	17.68	3.83	17.19	24.40	20.44	2.24
	III	9.18	16.30	11.16	1.72	9.07	16.41	11.83	2.00

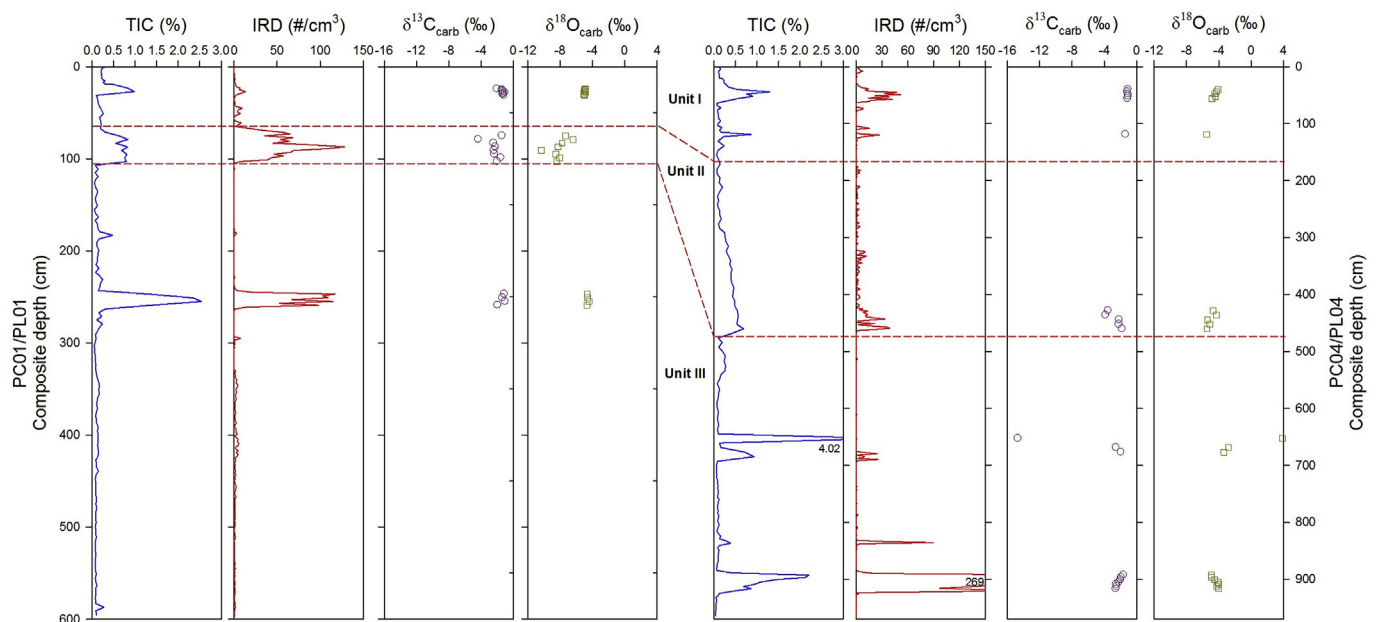


Fig. 6. Downcore profiles of the TIC content, IRD (ice-rafted debris) abundance, and $\delta^{13}\text{C}_{\text{carb}}$ (‰) and $\delta^{18}\text{O}_{\text{carb}}$ (‰) value of the bulk sediments and their correlation between two composite cores.

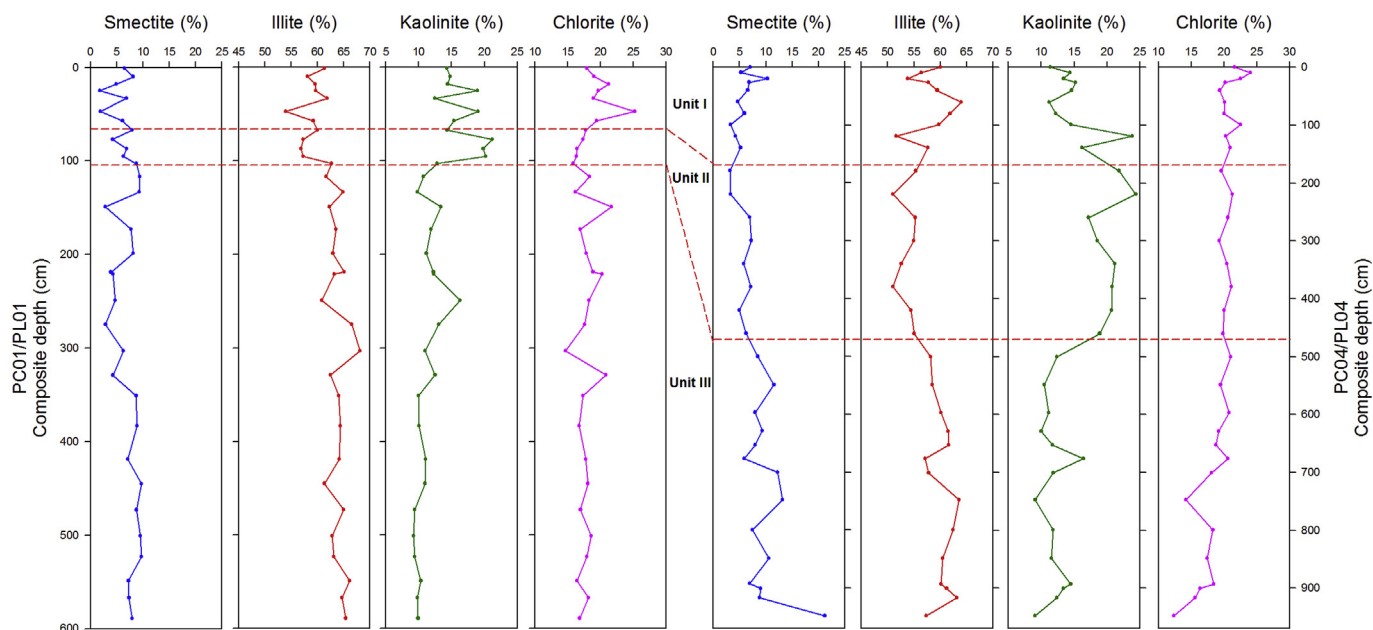


Fig. 7. Downcore profiles of four major clay minerals (smectite, illite, kaolinite, and chlorite) and their correlation between the two composite cores.

sediment starvation or even hiatus was observed in the deep sea basins (Darby et al., 1997; Polyak et al., 2004, 2009). The glacial pelagic sediments are generally olive gray to yellowish in color, with scant microfossils, fine-grained size and a very low

sedimentation rate (Polyak et al., 2009; Stein et al., 2010). Glacio-genic diamictos and glacial erosion on the seafloor were recognized dominantly in the shallow marine areas such as continental margins and submarine plateaus (Polyak et al., 2001, 2007; O'Regan

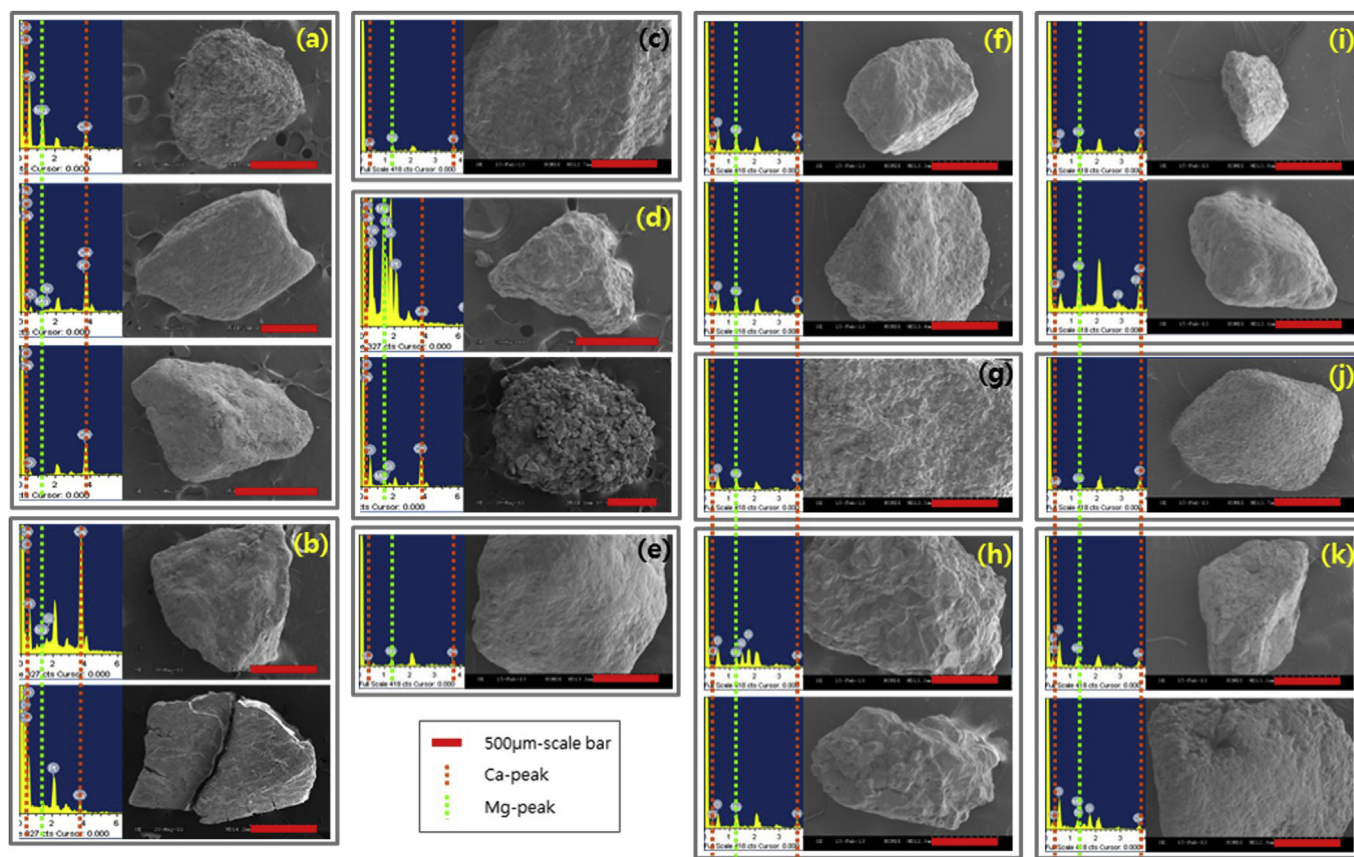


Fig. 8. SEM images and SEM-EDS result of the IRDs. Ca and Mg peaks are represented as the dotted orange and green lines, respectively. Scale bar (red line) represents 500 μm. Each gray-lined box means the samples of the same depth: (a) 77 cm, (b) 95 cm, (c) 199 cm, (d) 249 cm, and (e) 549 cm for PC01/PL01 and (f) 40 cm, (g) 60 cm, (h) 119 cm, (i) 676.7 cm, (j) 892.7 cm, and (k) 916.7 cm for PC04/PL04. (For interpretation of the references to colour in this figure legend, the reader is referred to the web version of this article.)

et al., 2008; Jakobsson et al., 2008, 2010; Dove et al., 2014). These glaciogenic diamictons were not observed in the present cores of our study (Fig. 3). During the deglacial periods when sea level rises, the exposed shelf areas were flooded, resulting in a modern appearing Arctic Ocean. This deglacial period is characterized by distinct deposition of coarse-grained IRD particles (Darby et al., 2006), as observed similarly in our cores (Figs. 3 and 4). Corresponding to Unit I in our cores, the interglacial (Holocene) sediments in the Arctic Ocean are usually brownish in color including abundant biological remains with a few IRD (Polyak et al., 2004; McKay et al., 2008; Adler et al., 2009).

Paleoceanographic proxies of the last glacial period (Unit III) indicate a decrease in marine productivity and terrigenous supply presumably under the thick sea ice conditions during the last glacial period. The limited surface water production due to the prevailed thick sea ice during the glacial periods is a main cause for the dominance of the terrigenous organic matter (Darby et al., 2006; Bradley and England, 2008). The organic geochemical properties (TOC, C/N, and $\delta^{13}\text{C}_{\text{org}}$; Fig. 5) within the deglacial interval (Unit II) indicate a greater input of terrestrial organic matter than the increase in marine productivity. The high TOC contents together with high C/N ratio and low $\delta^{13}\text{C}_{\text{org}}$ values in the Arctic marine sediments are interpreted to be related more to a terrigenous supply than to an increase in marine productivity (Stein et al., 1994; Schubert and Stein, 1996). On the contrary to the deglacial period, Unit I shows that the Chukchi Rise was more influenced by the marine environment under a high sea level stand at the end of deglaciation. Unit I of the two cores showed a distinct increase in TOC content (Fig. 5), which is consistent with the previous results in the Arctic Ocean (Naidu et al., 2004; Macdonald et al., 2004). Along with the TOC contents, an increase in the $\delta^{13}\text{C}_{\text{org}}$ values and a decrease in the C/N ratio in Unit I indicate enhanced marine productivity in the surface water during the middle to late Holocene (Fig. 5). Similar Holocene features have also been reported in many other areas of the Arctic Ocean (e.g., Stein et al., 1994; Schubert and Stein, 1996; Mueller-Lupp et al., 2000), in which the increase of primary productivity in surface water is a result of a lessened sea ice cover.

Concerning on the marine primary production, low and near-constant biogenic opal contents of Unit II and III (5% in average; Fig. 5) may reflect low biogenic opal (or diatom) productivity at the time of thick sea ice condition and, hence, diatom productivity was low during the last glacial and deglacial periods, as discussed above, although dilution effect by high terrigenous input cannot be ignored. On the other hand, the variation pattern of the biogenic opal contents between cores PC01 and PC04 was not similar during the late Holocene (Fig. 5). Such a difference might be caused by the geographical location which is related to the ice marginal zone. This suggests that core PC04/PL04 was influenced more by the seasonal variations of sea ice cover than the core PC01/PL01, presumably because of its latitudinal position (Fig. 1). Because primary production in surface waters is limited by sea ice and subsequent light penetration (Arrigo et al., 2008), the position of the sea ice marginal zone is important for the degree of surface water production. In addition, the more proximal location of core PC04/PL04 to the Chukchi Shelf is another factor for the difference of biogenic opal content because the productivity was higher close to the Chukchi Shelf than the Canadian Basin (Lee et al., 2012). Thus, the biogenic opal contents of core PC04/PL04 showed a more distinct increasing trend during the late Holocene (Fig. 5). Although different preservation of biogenic opal due to dissolution and/or diagenesis cannot be ruled out, core PC04 clearly indicates an increase in diatom productivity during the late Holocene when considering low C/N ratios and high TOC and $\delta^{13}\text{C}_{\text{org}}$ values (Fig. 5).

Aside from a distinct and thick IRD layer consisting of entire Unit

II, a few IRD layers were also preserved within Unit I and III (Figs. 3 and 4). It is worthy of note that all IRD layers of cores PC01 and PC04 coincide with the high TIC contents (Fig. 6). IRD layers in Unit I were deposited before an increase in diatom productivity (i.e., biogenic opal content) during the Holocene (Figs. 3–5). The IRDs in Unit I might have been transported by sea ice because the Laurentide Ice Sheet (LIS) on the Canadian Arctic Archipelago (CAA) was extinct completely at about 7–8 ka (Andrews et al., 1995). Darby et al. (1997) reported that the IRD event in the western Arctic Ocean during 3.5 to 1.5 ka might correspond to Neoglaciation in the North Atlantic. In contrast, the IRD layers during the glacial periods (Unit III) in the Arctic marine sediments are related to iceberg discharge events from the adjacent ice sheets (Bischof et al., 1996; Darby et al., 2002). For example, iceberg discharges in association with Heinrich events resulted in distinct IRD deposits in the western Arctic Ocean (Phillips and Grantz, 2001; Stokes et al., 2005). These IRD layers in the western Arctic Ocean generally contain large amount of detrital carbonate particles and the source of these detrital carbonates has been suggested to be the Banks and Victoria Islands (CAA) (Bischof et al., 1996; Darby et al., 2002; Stokes et al., 2005). In contrast to the dominant occurrence of detrital carbonate clasts in the western Arctic Ocean sediments, quartz particles derived mainly from the Barents-Kara Ice Sheet were the principal IRD components in the eastern Arctic Ocean sediments (Phillips and Grantz, 2001). The high TIC content of IRD peaks (Fig. 6), SEM-EDS observation of IRDs (Fig. 8), and lack of biogenic remnants indicate that almost all the carbonates in the sediments of the two cores are detrital. Thus, the detrital carbonates composed of IRD particles of the two cores show the sediment delivery by iceberg calving from the northern part of North America to the Chukchi Rise following the main path of the Beaufort Gyre.

$\delta^{18}\text{O}_{\text{carb}}$ and $\delta^{13}\text{C}_{\text{carb}}$ values of the bulk sediments in the two cores are almost consistent among the units except Unit II (Fig. 6). This suggests that these bulk carbonates may originate from a similar source, although the slightly lower $\delta^{18}\text{O}_{\text{carb}}$ values of Unit II in core PC01 might be due to the effect of freshwater diagenesis as a result of the large amount of meltwater discharge during the deglacial period (Fairchild et al., 1993). It is notable that an IRD horizon at 652.7 cm of core PC04/PL04 exhibited an abnormally low $\delta^{13}\text{C}_{\text{carb}}$ value (−14.7‰) and comparatively high $\delta^{18}\text{O}_{\text{carb}}$ value (3.9‰) (Fig. 6). Such extreme depletion of ^{13}C and enrichment of ^{18}O are the result of early diagenetic carbonate related to the bacterial oxidation of methane (Claypool and Kaplan, 1974). Cretaceous chemosynthetic carbonate mounds are distributed widely in Canadian Arctic regions (Beauchamp and Savard, 1992). Thus, isotopic signature of detrital carbonates also confirms that the IRD particles in the Chukchi Rise originated from the northern part of the North America.

Clay mineral composition of the fine-grained clastic particles was used to identify the sediment sources in the Arctic Ocean (Darby, 1975; Stein et al., 1994; Nürnberg et al., 1995; Wahsner et al., 1999; Dethleff et al., 2000; Khim, 2003; Yurco et al., 2010; Nwaodua et al., 2014). Illite is commonly widespread in almost all shelf areas except for the Kara Sea (Wahsner et al., 1999). In contrast, the distribution of smectite and kaolinite in the Arctic Ocean is influenced by their restricted source areas. For example, smectite, which is weathering product of the flood basalt of the Putoran Massif on the Siberian Platform, is transported by the Ob, Yenisei, and Katanga rivers into the Kara Sea (Nürnberg et al., 1995). Thus, the smectite contents in the Kara Sea are quite high (~40%), compared to the other regions in the Arctic Ocean (Stein et al., 1994). Similarly, the sources of kaolinite in the Arctic Ocean are confined to certain areas exposed by kaolinite-bearing rocks such as (1) the northern coasts of Alaska and Canada (Darby, 1975; Naidu and Mowatt, 1983), (2) the Svalbard and some shallow banks in the Barents

Sea (Wahsner et al., 1999), and (3) Franz-Josef Land (Nürnberg et al., 1995). Stein et al. (1994) suggested that sediments enriched in kaolinite in the Nansen Basin, east of Svalbard, and the Barents Sea were derived from the Mesozoic sediments in the Barents Sea and Franz-Josef Land in the Eurasian Arctic. Nevertheless, because the Beaufort Gyre is limited to the Canadian Basin, kaolinite in the Canadian Basin was most likely to have been derived from the northern part of North America. Thus, the high kaolinite content of Unit II (Fig. 7) indicate that the clay particles were transported by iceberg drift and/or meltwater discharge from the northern North America during the last deglacial period, because IRDs composed of detrital carbonate particles were delivered by the same trajectory.

4.2. Paleoceanographic implications of the thick glacial mud deposit in the Chukchi Rise

The Arctic Ocean experienced a sediment-starved condition during the glacial periods (Darby et al., 2006), indicating that surface productivity and input of terrigenous particles were limited by very thick perennial sea ice or even an extended ice shelf, resulting in very low sedimentation rates. Cores PC01/PL01 and PC04/PL04 in the Chukchi Rise, however, revealed very high sedimentation rates (more than 30 cm/kyr) during the last glacial period, compared to the average sedimentation rates (few cm per kilo-year) of the continental margins in the western Arctic Ocean during the Late Quaternary (Darby et al., 2006; Polyak et al., 2009; Stein et al., 2010). In the Arctic Ocean, high sedimentation rates (a few cm/kyr to m/kyr) are sometimes recorded in the continental margins and deep sea basins, where sediment mass wasting occurred (Grantz et al., 1996; Dowdeswell et al., 1998; Dowdeswell and Ó Cofaigh, 2002; Svindland and Vorren, 2002). Such an abrupt and instant sedimentation is normally accompanied with a large amount of coarse-grained sediment deposit. Grantz et al. (1996) reported that poorly-sorted coarse-grained turbidites with very high sedimentation rate (ca. 1.2 m/kyr) were deposited in the southern Canada Abyssal Plain. The core sediments of high sedimentation rate (up to 24.7 cm/kyr) in the Amundsen Basin were also attributed to turbidite deposition (Svindland and Vorren, 2002).

The glacial interval (Unit III) of cores PC01/PL01 and PC04/PL04 consisted mostly of massive or laminated mud with intercalated IRD layers (Figs. 3 and 4), which is different from the general mass wasting process including gravity flow. The IRD-rich layers (Unit II) and intercalated IRD layer in Unit I and III were characterized by high sand content (8.4–15.9%) and large mean grain size (7.0–12.4 μm), whereas thick mud deposit in Unit III shows low sand content (0.0–1.6%) and low mean grain size (4.3–5.8 μm) (Fig. 3). Under the glaciomarine environment, such fine-grained sediments could be deposited predominantly by meltwater-derived suspension and/or tidal pumping (Ó Cofaigh and Dowdeswell, 2001; Kilfeather et al., 2011). Thus, the fine-grained muds with low sand content of Unit III was most likely deposited by suspension settling, not by the distal stage of turbidity current. The glacier-influenced region receives a large amount of meltwater and sediment from the ice margin, resulting in ice-proximal high sedimentation rates (Cai et al., 1997), which also suggests that the thick mud deposit of Unit III was influenced by glaciogenic sedimentary condition. Ó Cofaigh and Dowdeswell (2001) suggested that the sediment lamination of fine-grained particle deposition results from suspension settling from meltwater plumes and slit/clay ratio decreases with the distance from the ice margin. In addition, preservation of sediment lamination diminished with increasing distance from the ice margin (Boulton, 1990; Cai et al., 1997). The lamination in the thick mud deposit of Unit III is another evidence for the fine-grained sediment deposition by

meltwater plume in the distal area from the ice margin (Ó Cofaigh and Dowdeswell, 2001). Thus, the thick glacial mud in Unit III was deposited in an ice-distal sedimentary environment of the Chukchi Rise.

Polyak et al. (2007) reported that diamictos in the Northwind Ridge were deposited directly by glaciers under the subglacial environments. On the other hand, fine-grained muddy sediments were observed directly above the diamictos and showed the reversed age, suggesting that these muddy sediments were deposited under aquatic depositional environments such as floating ice masses. The thick glacial mud of Unit III in this study might have been also deposited gradually from the continuous supply of fine silt-sized particles under the aquatic depositional environments (e.g., Powell and Domack, 1995). The age reversal of Unit III also supports continuous sediment supply by meltwater flux eroded from the young uppermost deposit and subsequently old lower deposit (Fig. 3). Jakobsson et al. (2008) observed the widespread glacial erosions on the seafloor of the Chukchi Borderland and demonstrated that these erosions might have been caused by two mechanisms: (1) grounding by floating ice masses (or ice shelves) originated from the LIS and (2) impact of an ice cap located in the Chukchi Plateau or the Borderland. Dove et al. (2014) also recognized many erosional bedforms grounded by glacier in the adjacent margins which occurred during the LGM in the water depths of shallower than 350 m. Our core site is deeper than 350 m, indicating the possible effect from the presence of ice in the Chukchi Shelf. Given that cores PC01 and PC04 preserve thick mud layer in Unit III except for the intercalated IRD layer (Figs. 3 and 4), Unit III seems to be affected by glacial meltwater plume which supplies mud-sized particles, not directly by ice-grounding activities or gravity flow which delivers coarser (sandy) and unsorted sediments, even by the final stage of turbidity current. Therefore, the anomalously thick glacial mud (Unit III) of our two cores showing the reversed age, which was deposited presumably by the continuous supply of suspension load, supports the possible presence of ice masses, such as an ice cap, ice shelf, or even ice sheet, near the Chukchi Rise during the last glacial period.

The most important characteristic of the Arctic environments during the Late Quaternary is the changes in cryosphere represented as the extent of the ice sheets and ice shelves (Denton et al., 2010). Large parts of the high-latitude landmasses in the Northern Hemisphere were occupied by huge continental ice sheets such as North American Ice Sheet and Eurasian Ice Sheet during the glacial periods (Ehlers and Gibbard, 2007). The presence of continental ice sheets is known relatively well in terms of its scale and distribution, but studies on the existence of marine-based ice sheets are controversial (Spielhagen et al., 2004; Jakobsson et al., 2013). For example, Hughes et al. (1977) suggested that all of the continental shelves in the Arctic Ocean even including the East Siberian Sea and Chukchi Sea were glaciated. In contrast, these broad continental shelves have been recognized as insignificant glaciation centers (Dove et al., 2014), although glaciogenic seafloor features implying ice arrival from the ice sheets were observed distinctly on the submarine ridges such as Lomonosov Ridge and Chukchi Boarderland (Jakobsson et al., 2008, 2010). The latest evidence of a glaciogenic morphology proved a widespread grounded-ice presence on the northern Chukchi Shelf; however, the initiation age of the glacial impact on this area is not yet constrained (Dove et al., 2014). Thus, further studies on the glaciogenic sediments for the presence of an ice shelf or ice sheet in the Chukchi margin will be needed.

5. Conclusions

The three lithologic units (Unit I, Unit II, and Unit III) of two composite cores (PC01/PL01 and PC04/PL01) collected from the

Chukchi Rise recorded the paleoenvironmental changes since the last glacial period. These three lithologic units, corresponding to the three temporal intervals (last glacial, deglacial, and Holocene), were also differentiated distinctly by the diverse sediment properties, such as geochemical and mineralogical data. Unit III was characterized by high sedimentation rates during the last glacial period, compared to the other regions in the western Arctic Ocean. Such thick glacial mud deposits might have been related to the consistent supply of fine-grained particles by meltwater-derived suspension and/or tidal pumping under the ice-distal depositional conditions. Thus, Unit III implies the probable presence of stable ice masses (e.g., ice cap, ice shelf, or even small ice sheet) in the Chukchi margin. Unit II was characterized by distinct geochemical and mineralogical features during the last deglacial period. Geochemical and mineralogical data indicated the sediment provenance and pathways of IRDs and clay minerals, suggesting that these coarse- and fine-grained sediments are transported from the northern North America by the dominant role of the Beaufort Gyre. The geochemical properties of Unit I show that the marine environmental condition has been stronger in the Chukchi Rise since the end of deglaciation, based on the increase in marine diatom productivity and the decrease in terrigenous input.

Acknowledgements

We would like to thank captain, crews and all onboard researchers of MR09-03 cruise by R/V Mirai of JAMSTEC for their assistance in core sampling. We also appreciate Dr. Leonid Polyak (Byrd Polar Research Center) on his fruitful comments to improve the lithostratigraphic establishment and two anonymous reviewers for their critical and constructive comments to improve the interpretation. This research was supported by the Polar Academic Program (PAP) of the Korea Polar Research Institute, the Korea-Polar Ocean in Rapid Transition (K-PORT; PM13020) Program of the Ministry of Oceans and Fisheries (Korea), and JSPS KAKENHI Grant Number 20310011.

Appendix A. Supplementary data

Supplementary data related to this article can be found at <http://dx.doi.org/10.1016/j.polar.2017.01.002>.

References

- Abdalati, W., Steffen, K., 2001. Greenland ice sheet melt extent: 1979–1999. *J. Geophys. Res. (Atmos.)* 106, 33983–33988.
- Adler, R.E., Polyak, L., Ortiz, J.D., Kaufman, D.S., Channell, J.E., Xuan, C., Grotto, A.G., Sellén, E., Crawford, K.A., 2009. Sediment record from the western Arctic Ocean with an improved late quaternary age resolution: HOTRAX core HLY0503-8JPC, mendeleev ridge. *Glob. Planet. Change* 68, 18–29.
- Andrews, J.T., Maclean, B., Kerwin, M., Manley, W., Jennings, A.E., Hall, F., 1995. Final stages in the collapse of the Laurentide ice sheet, Hudson Strait, Canada, NWT: ^{14}C AMS dates, seismic stratigraphy, and magnetic susceptibility logs. *Quat. Sci. Rev.* 14, 983–1004.
- Arrigo, K.R., van Dijken, G., Pabi, S., 2008. Impact of a shrinking Arctic ice cover on marine primary production. *Geophys. Res. Lett.* 35, L19603. <http://dx.doi.org/10.1029/2008GL035028>.
- Backman, J., Jakobsson, M., Frank, M., Sangiorgi, F., Brinkhuis, H., Stickley, C., O'Regan, M., Løvlie, R., Pålke, H., Spofforth, D., Gattacecca, J., Moran, K., King, J., Heil, C., 2008. Age model and core-seismic integration for the cenozoic arctic coring expedition sediments from the Lomonosov Ridge. *Paleoceanography* 23, PA1503. <http://dx.doi.org/10.1029/2007PA001476>.
- Backman, J., Jakobsson, M., Løvlie, R., Polyak, L., Febo, L.A., 2004. Is the central Arctic Ocean a sediment starved basin? *Quat. Sci. Rev.* 23, 1435–1454.
- Beauchamp, B., Savard, M., 1992. Cretaceous chemosynthetic carbonate mounds in the Canadian Arctic. *Palaios* 7, 434–450.
- Biscaye, P.E., 1964. Distribution between kaolinite and chlorite in recent sediments by x-ray diffraction. *Am. Mineral.* 49, 1281–1289.
- Biscaye, P.E., 1965. Mineralogy and sedimentation of recent deep-sea clay in the Atlantic Ocean and adjacent seas and oceans. *Geol. Soc. Am. Bull.* 76, 803–832.
- Bischof, J., Clark, D.L., Vincent, J.S., 1996. Origin of ice-rafted debris: pleistocene paleoceanography in the western Arctic Ocean. *Paleoceanography* 11, 743–756.
- Blott, S.J., Pye, K., 2001. GRADISTAT: a grain size distribution and statistics package for the analysis of unconsolidated sediments. *Earth Surf. Proc. Land* 26, 1237–1248.
- Boulton, G.S., 1990. Sedimentary and sea level changes during glacial cycles and their control on glacial marine facies architecture. In: Dowdeswell, J.D., Scourse, J.A. (Eds.), *Glaciomarine Environments: Processes and Sediments*, vol. 53. *Geol. Soc. London Spec. Publ.*, pp. 15–52.
- Bradley, R.S., England, J.H., 2008. The Younger Dryas and the sea of ancient ice. *Quat. Res.* 70, 1–10.
- Brunton, G., 1955. Vapor pressure glycolation of oriented clay minerals. *Am. Mineral.* 40, 124–126.
- Cai, J., Powell, R.D., Cowan, E.A., Carlson, P.R., 1997. Lithofacies and seismic-reflection interpretation of temperate glacial marine sedimentation in Tarr Inlet, Glacier Bay, Alaska. *Mar. Geol.* 143, 5–37.
- Callaghan, T.V., Johansson, M., Key, J., Prowse, T., Ananicheva, M., Klepikov, A., 2011. Feedbacks and interactions: from the Arctic cryosphere to the climate system. *Ambio* 40, 75–86.
- Claypool, G.E., Kaplan, I.R., 1974. The origin and distribution of methane in marine sediments. In: Kaplan, I.R. (Ed.), *Natural Gases in Marine Sediments*. Plenum, New York, pp. 99–139.
- Cowan, E.A., Seramur, K.C., Cai, J., Powell, R.D., 1999. Cyclic sedimentation produced by fluctuations in meltwater discharge, tides and marine productivity in an Alaskan fjord. *Sedimentology* 46, 1109–1126.
- Darby, D.A., 1975. Kaolinite and other clay minerals in Arctic Ocean sediments. *J. Sediment. Res.* 45, 272–279.
- Darby, D.A., Bischof, J.F., Jones, G.A., 1997. Radiocarbon chronology of depositional regimes in the western Arctic Ocean. *Deep-Sea Res. II* 44, 1745–1757.
- Darby, D.A., Bischof, J.F., Spielhagen, R.F., Marshall, S.A., Herman, S.W., 2002. Arctic ice export events and their potential impact on global climate during the late Pleistocene. *Paleoceanography* 17, 1025. <http://dx.doi.org/10.1029/2001PA000639>.
- Darby, D.A., Polyak, L., Bauch, H.A., 2006. Past glacial and interglacial conditions in the Arctic Ocean and marginal seas—a review. *Prog. Oceanogr.* 71, 129–144.
- Denton, G.H., Anderson, R.F., Toggweiler, J.R., Edwards, R.L., Schaefer, J.M., Putnam, A.E., 2010. The last glacial termination. *Science* 328, 1652–1656.
- Dethleff, D., Rachold, V., Tinteln, M., Antonow, M., 2000. Sea-ice transport of riverine particles from the Laptev Sea to Fram Strait based on clay mineral studies. *Int. J. Earth Sci.* 89, 496–502.
- Dove, D., Polyak, L., Coakley, B., 2014. Widespread, multi-source glacial erosion on the Chukchi margin, Arctic Ocean. *Quat. Sci. Rev.* 92, 112–122.
- Dowdeswell, J.A., Ó Cofaigh, C., 2002. Glacier-influenced sedimentation on high-latitude continental margins: introduction and overview. In: Dowdeswell, J.A., Ó Cofaigh, C. (Eds.), *Glacier-influenced Sedimentation on High-latitude Continental Margins*, vol. 203. *Geol. Soc. London Spec. Publ.*, pp. 1–9.
- Dowdeswell, J.A., Elverhfi, A., Spielhagen, R., 1998. Glacial marine sedimentary processes and facies on the Polar North Atlantic margins. *Quat. Sci. Rev.* 17, 243–272.
- Ehlers, J., Gibbard, P.L., 2007. The extent and chronology of Cenozoic global glaciation. *Quat. Int.* 164, 6–20.
- Fairchild, I.J., Bradby, L., Spiro, B., 1993. Carbonate diagenesis in ice. *Geology* 21, 901–904.
- Grantz, A., Phillips, R.L., Mullen, M.W., Starratt, S.W., Jones, G.A., Naidu, A.S., Finney, B.P., 1996. Character, paleoenvironment, rate of accumulation, and evidence for seismic triggering of Holocene turbidites, Canada Abyssal Plain, Arctic Ocean. *Mar. Geol.* 133, 51–73.
- Hanslik, D., Jakobsson, M., Backman, J., Björck, S., Sellén, E., O'Regan, M., Fornaciari, E., Skog, G., 2010. Quaternary Arctic Ocean sea ice variations and radiocarbon reservoir age corrections. *Quat. Sci. Rev.* 29, 3430–3441.
- Hughes, T., Denton, G.H., Grosswald, M.G., 1977. Was there a late-Würm Arctic ice sheet. *Nature* 266, 596–602.
- Intergovernmental Panel on Climate Change, 2007. Summary for policymakers. In: Solomon, S. (Ed.), *Climate Change 2007-The Physical Science Basis. Contribution of Working Group I to the Fourth Assessment Report of the Intergovernmental Panel on Climate Change*. Cambridge University Press, Cambridge and New York, p. 18.
- Jakobsson, M., Andreassen, K., Bjarnadóttir, L.R., Dove, D., Dowdeswell, J.A., England, J.H., Funder, S., Hogan, K., Ingólfsson, Ó., Jennings, A., Larsen, N.K., Kirchner, N., Landvik, J.Y., Mayer, L., Mikkelsen, Naja, Möller, P., Niessen, F., Nilsson, J., O'Regan, M., Polyak, L., Nørgaard-Pedersen, N., Stein, R., 2013. Arctic Ocean glacial history. *Quat. Sci. Rev.* 92, 40–67.
- Jakobsson, M., Polyak, L., Edwards, M., Kleman, J., Coakley, B., 2008. Glacial geomorphology of the central Arctic Ocean: the Chukchi Borderland and the Lomonosov Ridge. *Earth Surf. Proc. Land* 33, 526–545.
- Jakobsson, M., Nilsson, J., O'Regan, M., Backman, J., Löwemark, L., Dowdeswell, J.A., Mayer, L., Polyak, L., Colleoni, F., Anderson, L.G., Björck, G., Darby, D.A., Eriksson, B., Hanslik, D., Hell, B., Marcussen, C., Sellén, E., Wallin, A., 2010. An Arctic Ocean ice shelf during MIS 6 constrained by new geophysical and geological data. *Quat. Sci. Rev.* 29, 3505–3517.
- Jones, B.M., Arp, C.D., Jorgenson, M.T., Hinkel, K.M., Schmutz, J.A., Flint, P.L., 2009. Increase in the rate and uniformity of coastline erosion in Arctic Alaska. *Geophys. Res. Lett.* 36, L03503. <http://dx.doi.org/10.1029/2008GL036205>.
- Kilfeather, A.A., Cofaigh, C.O., Lloyd, J.M., Dowdeswell, J.A., Xu, S., Moreton, S.G., 2011. Ice-stream retreat and ice-shelf history in marguerite trough, antarctic peninsula: sedimentological and foraminiferal signatures. *Geol. Soc. Am. Bull.*

- 123, 997–1015.
- Khim, B.K., 2003. Two modes of clay-mineral dispersal pathways on the continental shelves of the East Siberian Sea and western Chukchi Sea. *Geosci. J.* 7, 253–262.
- Lawrence, D.M., Slater, A.G., Tomas, R.A., Holland, M.M., Deser, C., 2008. Accelerated Arctic land warming and permafrost degradation during rapid sea ice loss. *Geophys. Res. Lett.* 35, L11506. <http://dx.doi.org/10.1029/2008GL033985>.
- Lee, S.H., Joo, H.M., Liu, Z., Chen, J., He, J., 2012. Phytoplankton productivity in newly opened waters of the Western Arctic Ocean. *Deep-Sea Res. II* 81, 18–27.
- Macdonald, R.W., Naidu, A.S., Yunker, M.B., Gobeil, C., 2004. The Beaufort Sea: distribution, sources, fluxes and burial of organic carbon. In: Stein, R., Macdonald, R.W. (Eds.), *The Organic Carbon Cycle in the Arctic Ocean*. Springer Publishing Company, Berlin, pp. 177–192.
- McKay, J.L., de Vernal, A., Hillaire-Marcel, C., Not, C., Polyak, L., Darby, D., 2008. Holocene fluctuations in Arctic sea ice cover: dinocyst-based reconstructions for the eastern Chukchi Sea. *Can. J. Earth Sci.* 45, 1377–1397.
- Mortlock, R.A., Froelich, P.N., 1989. A simple method for the rapid determination of biogenic opal in pelagic marine sediments. *Deep-Sea Res.* 36, 1415–1426.
- Mueller-Lupp, T., Bauch, H.A., Erlenkeuser, H., Hefter, J., Kassens, H., Thiede, J., 2000. Changes in the deposition of terrestrial organic matter on the Laptev Sea shelf during the Holocene: evidence from stable carbon isotopes. *Int. J. Earth Sci.* 89, 563–568.
- Naidu, A.S., Mowatt, T.C., 1983. Sources and dispersal patterns of clay minerals in surface sediments from the continental-shelf areas off Alaska. *Geol. Soc. Am. Bull.* 94, 841–854.
- Naidu, A.S., Cooper, L.W., Grebmeier, J.M., Whitley, T.E., Hameedi, M.J., 2004. The continental margin of the North Bering-Chukchi Sea: concentrations, sources, fluxes, accumulation and burial rates of organic carbon. *Mar. Geol.* 119, 185–214.
- Nwaodua, E.C., Ortiz, J.D., Griffith, E.M., 2014. Diffuse spectral reflectance of surficial sediments indicates sedimentary environments on the shelves of the Bering Sea and western Arctic. *Mar. Geol.* 355, 218–233.
- Nürnberg, D., Levitan, M.A., Pavlidis, J.A., Shelekhova, E.S., 1995. Distribution of clay minerals in surface sediments from the eastern Barents and south-western Kara seas. *Geol. Rundsch* 84, 665–682.
- O'Regan, M., King, J., Backman, J., Jakobsson, M., Pälike, H., Moran, K., Heil, C., Sakamoto, T., Cronin, T.M., Jordan, R.W., 2008. Constraints on the pleistocene chronology of sediments from the Lomonosov Ridge. *Paleoceanography* 23, PA1S19. <http://dx.doi.org/10.1029/2007PA001551>.
- Ó Cofaigh, C., Dowdeswell, J.A., 2001. Laminated sediments in glaci-marine environments: diagnostic criteria for their interpretation. *Quat. Sci. Rev.* 20, 1411–1436.
- Peterson, B.J., Holmes, R.M., McClelland, J.W., Vorosmarty, C.J., Lammers, R.B., Shiklomanov, A.I., Shiklomanov, I.A., Rahmstorf, S., 2002. Increasing river discharge to the Arctic Ocean. *Science* 298, 2171–2173.
- Phillips, R.L., Grantz, A., 2001. Regional variations in provenance and abundance of ice-rafted clasts in Arctic Ocean sediments: implications for the configuration of late Quaternary oceanic and atmospheric circulation in the Arctic. *Mar. Geol.* 172, 91–115.
- Polyak, L., Edwards, M.H., Coakley, B.J., Jakobsson, M., 2001. Ice shelves in the Pleistocene Arctic Ocean inferred from glaciogenic deep-sea bedforms. *Nature* 410, 453–457.
- Polyak, L., Curry, W.B., Darby, D.A., Bischof, J., Cronin, T.M., 2004. Contrasting glacial/interglacial regimes in the western Arctic Ocean as exemplified by a sedimentary record from the Mendeleev Ridge. *Palaeogeogr. Palaeoclimatol. Palaeoecol.* 203, 73–93.
- Polyak, L., Darby, D.A., Bischof, J.F., Jakobsson, M., 2007. Stratigraphic constraints on late Pleistocene glacial erosion and deglaciation of the Chukchi margin, Arctic Ocean. *Quat. Res.* 67, 234–245.
- Polyak, L., Bischof, J., Ortiz, J.D., Darby, D.A., Channell, J.E., Xuan, C., Kaufman, D.S., Lovlie, R., Schneider, D.A., Eberl, D.D., Adler, R.E., Council, E.A., 2009. Late Quaternary stratigraphy and sedimentation patterns in the western Arctic Ocean. *Glob. Planet. Change* 68, 5–17.
- Polyak, L., Jakobsson, M., 2011. Quaternary sedimentation in the Arctic Ocean: recent advances and further challenges. *Oceanography* 24, 52–64.
- Powell, R.D., Domack, E., 1995. Modern glaci-marine environments. In: Menzies, J. (Ed.), *Modern Glacial Environments: Processes, Dynamics and Sediments*. Butterworth-Heinemann, Boston, MA, pp. 445–486.
- Reimer, P.J., Baillie, M.G., Bard, E., Bayliss, A., Beck, J.W., Blackwell, P.G., Bronk Ramsey, C., Buck, C.E., Burr, G.S., Edwards, R.L., Friedrich, M., Grootes, P.M., Guilderson, T.P., Hajdas, I., Heaton, T.J., Hogg, A.G., Hughen, K.A., Kaiser, K.F., Kromer, B., McCorman, F.G., Manning, S.W., Reimer, R.W., Richards, D.A., Southon, J.R., Talamo, S., Turney, C.S.M., van der Plicht, J., Weyhenmeyer, C.E., 2009. IntCal09 and Marine09 radiocarbon age calibration curves, 0–50,000 years cal BP. *Radiocarbon* 51, 1111–1150.
- Schubert, C.J., Stein, R., 1996. Deposition of organic carbon in Arctic Ocean sediments: terrigenous supply vs marine productivity. *Org. Geochem* 24, 421–436.
- Shimada, K., Kamoshida, T., Itoh, M., Nishino, S., Carmack, E., McLaughlin, F., Zimmermann, S., Proshutinsky, A., 2006. Pacific Ocean inflow: influence on catastrophic reduction of sea ice cover in the Arctic Ocean. *Geophys. Res. Lett.* 33, L08605. <http://dx.doi.org/10.1029/2005GL025624>.
- Spielhagen, R.F., Baumann, K.H., Erlenkeuser, H., Nowaczyk, N.R., Nørgaard-Pedersen, N., Vogt, C., Weiel, D., 2004. Arctic Ocean deep-sea record of northern Eurasian ice sheet history. *Quat. Sci. Rev.* 23, 1455–1483.
- Stein, R., Grobe, H., Wahsner, M., 1994. Organic carbon, carbonate, and clay mineral distributions in eastern central Arctic Ocean surface sediments. *Mar. Geol.* 119, 269–285.
- Stein, R., Matthiessen, J., Niessen, F., Krylov, A., Nam, S.I., Bazhenova, E., 2010. Towards a better (litho-) stratigraphy and reconstruction of Quaternary paleo-environment in the Amerasian Basin (Arctic Ocean). *Polarforschung* 79, 97–121.
- Stokes, C.R., Clark, C.D., Darby, D.A., Hodgson, D.A., 2005. Late pleistocene ice export events into the Arctic Ocean from the M'Clure Strait ice stream, Canadian Arctic Archipelago. *Glob. Planet. Change* 49, 139–162.
- Stokke, P.R., Carson, B., 1973. Variation in clay mineral X-ray diffraction results with the quantity of sample mounted. *J. Sediment. Res.* 43, 957–964.
- Stroeve, J.C., Serreze, M.C., Holland, M.M., Kay, J.E., Malanik, J., Barrett, A.P., 2012. The Arctic's rapidly shrinking sea ice cover: a research synthesis. *Clim. Change* 110, 1005–1027.
- Svindland, K.T., Vorren, T.O., 2002. Late cenozoic sedimentary environments in the Amundsen Basin, Arctic Ocean. *Mar. Geol.* 186, 541–555.
- Wahsner, M., Müller, C., Stein, R., Ivanov, G., Levitan, M., Shelekhova, E., Tarasov, G., 1999. Clay-mineral distribution in surface sediments of the Eurasian Arctic Ocean and continental margin as indicator for source areas and transport pathways—a synthesis. *Boreas* 28, 215–233.
- Wang, R., Xiao, W., Li, W., Sun, Y., 2010. Late quaternary ice-rafted detritus events in the Chukchi basin, western Arctic Ocean. *Chin. Sci. Bull.* 55, 432–440.
- Yurco, L.N., Ortiz, J.D., Polyak, L., Darby, D.A., Crawford, K.A., 2010. Clay mineral cycles identified by diffuse spectral reflectance in Quaternary sediments from the Northwind Ridge: implications for glacial–interglacial sedimentation patterns in the Arctic Ocean. *Polar Res.* 29, 176–197.